Earth and Planetary Science Letters 276 (2008) 314–322

Contents lists available at ScienceDirect

Earth and Planetary Science Letters

journal homepage: www.elsevier.com/locate/epsl

Does the Karakoram fault interrupt mid-crustal channel flow in the western Himalaya?

Mary L. Leech

Department of Geosciences, San Francisco State University, San Francisco, CA 94132, United States

ARTICLE INFO

Article history:
Received 1 July 2008
Received in revised form 7 October 2008
Accepted 8 October 2008
Available online 12 November 2008

Editor: R.W. Carlson

Keywords:
U-Pb SHRIMP
Zircon
Leo Pargil
Gniess dome
Leucogranite
Channel flow
Himalaya
Tibet
Karakoram fault
Miocene

ABSTRACT

Variations in the volume and age of Miocene granites and in mid-crustal conductance from the northwest Himalaya to southeastern Tibet imply lateral differences in late orogenic processes. The change from west to east occurs near the Gurla Mandhata dome, where the Karakoram fault terminates and merges with the Indus–Yarlung suture zone. The 'channel flow' model, developed in southeastern Tibet, predicts that anatectic partial melts beneath the Tibetan plateau are gravitationally-driven south to a topographic erosional front and are exposed as leucogranites in the Greater Himalaya Sequence; upwellings of these channel granites occur as gneiss domes in the Tethyan Himalaya Sequence. Published magnetotelluric profiles show high conductivity 30–40 km deep beneath Tibet from c. 400 km north of the Main Frontal thrust south across the suture zone, beneath the Himalayan gneiss domes, and to the topographic front; this conductive middle crust corresponds to 2–4% partial melt in the northwest Himalaya and 5–12% melt in southeastern Tibet, sufficient in the latter case to weaken rock for flow. East of the Karakoram termination leucogranites are abundant and are as young as 7 Ma; west of the termination, channel granites are less abundant and no younger than 18 Ma. Middle Miocene (16–14 Ma) leucogranites are found in the Karakoram fault zone located north of the suture zone and south of the proposed anatectic melt source. The initiation of motion on the crustal-penetrating Karakoram fault at 25–21 Ma may have created a barrier to the southward flow of mid-crustal melts and acted as a vertical conduit for these same melts.

1. Introduction

There is a marked change in the volume and age of granitoids from west to east across the Himalaya; that change occurs near the southeastern termination of the Karakoram fault where it merges with the Indus–Yarlung suture zone, near the Gurla Mandhata gneiss dome. Geologic transects through the Greater Himalayan Sequence (GHS) along the Beas and Sutlej River valleys in the western Himalaya near the Leo Pargil gneiss dome reveal rare to minimal amounts of migmatites and leucogranite compared to abundant migmatites and large leucogranite bodies in the area of the North Himalayan gneiss domes to the east, for example. Fig. 1 plots published crystallization ages for leucogranite bodies in the GHS and granites from gneiss domes within the Tethyan Himalaya Sequences (THS) along the length of the Himalaya; only Late Oligocene to Early Miocene granites occur west of the eastern termination of the Karakoram fault but granites range from Late Eocene to Late Miocene east of the termination.

Himalayan leucogranites are widely thought to be derived from a ductile mid-crustal channel formed when anatectic melts from the overthickened crust beneath the Tibetan plateau were gravitationally driven south by a pressure gradient to the Himalayan topographic front where focused, efficient erosion and concomitant shearing along the South Tibetan detachment (STD) and the Main Central thrust exhume channel rocks (e.g., Nelson et al., 1996; Beaumont et al., 2004; Godin et al., 2006; Grujic, 2006). Finite element models (Beaumont et al., 2004) predict upwellings of these granites within the THS as part of a chain of granitic gneiss domes (probably resulting from instabilities within the channel and the overburden; Grujic et al., 2002) and erosional exposure of the paleo-channel as the GHS as evidenced by widespread migmatites and leucogranite bodies in the footwall of the STD (Fig. 1, Beaumont et al., 2004; Godin et al., 2006; Grujic, 2006). Data presented here suggest that the Karakoram fault interrupted channel flow processes in the western Himalaya starting in the Early Miocene.

2. New ages for the Leo Pargil gneiss dome, western Himalaya

Leo Pargil is the westernmost granitic gneiss dome in the chain of domes formed within the THS that extends 1600 km eastward through the North Himalayan gneiss domes and includes the better-known Kangmar dome (Fig. 1; e.g., Lee et al., 2000). Because of the relative paucity of ages from granites west of Gurla Mandhata, the new dating presented here from the Leo Pargil granite allows comparison of ages west and east of the termination of the Karakoram fault. U–Pb

E-mail address: leech@sfsu.edu.

0012-821X/$ – see front matter © 2008 Elsevier B.V. All rights reserved.
doi:10.1016/j.epsl.2008.10.006

SHRIMP dating shows that zircons from leucogranites from the Leo Pargil gneiss dome are Late Oligocene to Early Miocene (27–19 Ma) corresponding to the older granites dated from the eastern Himalaya (Figs. 1 and 2, Tables 1 and 2).

A total of 93 zircon U–Pb SHRIMP analyses from 8 samples from the Leo Pargil gneiss dome yield Tertiary ages for igneous zircon domains (Fig. 2a); these analyses have high U contents (1000 to >25,000 ppm, Table 2), typical of Himalayan granitoids (e.g., Carosi et al., 2006). Zircon grains were separated and mounted using standard sample preparation methods for ion microprobe analysis (Williams, 1998). U–Pb SHRIMP analysis, *Squid* data reduction, and data plotting using *Isoplot* also followed standard techniques (Williams, 1998; Ludwig, 1999, 2001). Care was taken to make no morphologic or color differentiation during handpicking for grain sample mounts. Mounted zircons include euhedral, sub-rounded, and irregularly-shaped grains, some of which display clear core–mantle–rim zoning relationships while others are cloudy under cathodoluminescence imaging. Zircons were analyzed using the SHRIMP–RG (reverse-geometry) at the Stanford-U.S. Geological Survey Microanalysis center. U–Th–Pb data for each ~30 μm spot were collected in five scans and U–Pb ratios were calibrated with reference standard R33 (419 Ma; Black et al., 2004), which was analyzed after every fourth unknown analysis, and calibrated to CZ3 for U concentrations.

Linear regression of U content vs. age for all Tertiary data shows a trend toward younger ages from zircons with lower U contents (1000–3000 ppm) and that is consistent with lower intercept ages for individual samples (inset, Fig. 2a). The older apparent ages are likely a result of an instrumental effect from high U concentrations; at U concentrations >4000 ppm, there is non-linearity between Pb and U counts (seen as a deadtime correction for the electron multiplier) on the SHRIMP–RG that results in undercounting U and hence older apparent ages (J. Wooden and F. Mazdab, pers. comm.; Williams, 1998). Discounting zircon analyses with U concentrations over 4000 ppm and high common Pb (>2%, corresponding to the more discordant data in Fig. 2a) yields a spread of concordant or near-concordant ages (uncorrected for common Pb) from 27 to 19 Ma for Leo Pargil granites (Fig. 2b). This spread in crystallization ages (27–19 Ma) likely reflects multiple intrusive events and this interpretation of these U–Pb data is comparable to granites from the Ruby Mountains metamorphic core complex in the northern Basin and Range province (J. Wooden, pers. comm.). These Early Miocene granite ages are similar to other granitoids in the western Himalaya; in comparison, granites in the east are as young as Late Miocene (Fig. 1).

3. The Channel Flow model

Channel flow was originally conceived as ductile mid-crustal flow within a thermally-weakened channel resulting from partial melts in the overthickened crust beneath Tibet, recognized geologically as the extrusion of ductilely-deformed rocks of the GHS containing syntectonic leucogranites and bound by a normal-sense shear zone to the top (the STD) and south-directed ductile thrusting at its base along the Main Central thrust (Grujic et al., 1996). The first geophysical evidence for this partially-molten middle crust was extraordinary heat flow in southernmost Tibet (>500 mWm^{-2} in the NW Himalaya, Shanker et al., 1976; 91 mWm^{-2} and 146 mWm^{-2} near Kangmar dome, Francheteau et al., 1984), bright spots in seismic profiles of southern Tibet (Nelson et al., 1996), and anomalous electrically-conductive middle crust extending southward beneath the Indus–Yarlung suture zone to the Kangmar dome (Chen et al., 1996). The "channel flow" model of Nelson et al. (1996) made a direct physical connection between inferred mid-crustal melts in underthrust Indian and Lhasa terrane crust in southern Tibet and the Himalayan leucogranites that are exposed in the Greater Himalaya.

The channel flow model has evolved from the original concepts of Grujic et al. (1996) and Nelson et al. (1996) into a series of thermo-mechanical models (Beaumont et al., 2004, 2006; Jamieson et al., 2004). The main features of the models include: Indian upper crustal rocks are thrust under the Tethyan portion of the thrust belt and the southern part of the Tibetan Plateau, where they reach partial melting temperatures. Gravitational potential energy from the thick Tibetan crust drives the underthrust and partially molten rock southward in a ductile mid-crustal channel (Hodges, 2006; Hodges et al., 2001; Medvedev and Beaumont, 2006). Rapid Oligocene erosion advects the channel toward the surface, and the upper and lower walls of the channel are the active South Tibetan Detachment and Main Central thrust, respectively.

The Beaumont et al. (2004) model for channel flow requires a factor of 10 reduction in viscosity in the mid-crust for those rocks to flow, requiring melt fractions >5–7% (Rosenberg and Handy, 2005); this is the minimum amount of melt required to satisfy the magnetotelluric data for southeast Tibet near the Kangmar dome (5–12%, Gaillard et al., 2004; Unsworth et al., 2005) but is significantly higher than that for the northwest Himalaya near the Leo Pargil gneiss dome (2–4%, Unsworth et al., 2005).

4. Magnetotelluric implications for mid-crustal melts

Unsworth et al. (2005) suggest that the highly conductive middle crust inferred from four magnetotelluric (MT) transects from west to east across the Himalaya indicates that there is lateral continuity along the orogen implying that the volume of melt is sufficient for the channel flow process. These N–S MT profiles were located at ~77°E in the northwest Himalaya ('NW Him' in Fig. 1), ~85°E in Nepal (800 line), ~89–90°E along the INDEPTH I and II profiles (100 line), and ~92°E in eastern Tibet (700 line), and all cross the structural position of the north Himalayan domes, the Indus–Yarlung suture zone, and extend into the southern Tibetan plateau (Fig. 1). MT data show that the conductive middle crust extends to c. 400 km north of the Main Frontal thrust; Fig. 1 shows the approximate location of the channel melts at 30–40 km depth at this position in the Tibet plateau. Despite the continuity of this conductive layer, there is a marked difference in the conductivity in the northwest Himalaya profile, west of the Karakoram fault termination; this variation in conductivity results from a difference in the corresponding melt percentage: 2–4% partial melt in the NW Himalaya versus 5–12% melt for the three MT profiles in the eastern Himalaya (Unsworth et al., 2005). Rosenberg and Handy (2005) show that >5–7% melt reduces rock strength by an order of magnitude which corresponds to the amount of melt required by MT data for the eastern Himalaya. The much smaller melt percentage (2–4%) in the NW Himalaya may indicate insufficient melt for ductile flow and/or represent a lack of melt supply from beneath the Tibetan plateau. This interpretation is further supported by a recent analysis of broadband teleseismic body wave recordings that show a lack of a continuous low-velocity layer in the mid-crust in the west making channel flow unlikely (Oreshin et al., 2008).

5. Northern extent of underthrust Indian crust beneath Tibet and source of channel melts

Estimates for the northward reach of the Indian crust underneath the Tibetan plateau (i.e., the source of anatectic melts required for the channel flow model; Beaumont et al., 2004) vary widely depending on the geological or geophysical data used (Hoke et al., 2000; DeCelles et al., 2002; Kind et al., 2002; Klemperer, 2008; Bendick and Flesch, 2007; King et al., 2007). Kind et al. (2002) combine seismic datasets to image the subsurface structure beneath Tibet; these receiver function data show that the Indian crust extends north of the IYSZ beneath the Lhasa terrane to about 150 km south of the Bangong–Nujiang suture (Fig. 1). This corresponds to ^{3}He data from geothermal areas in

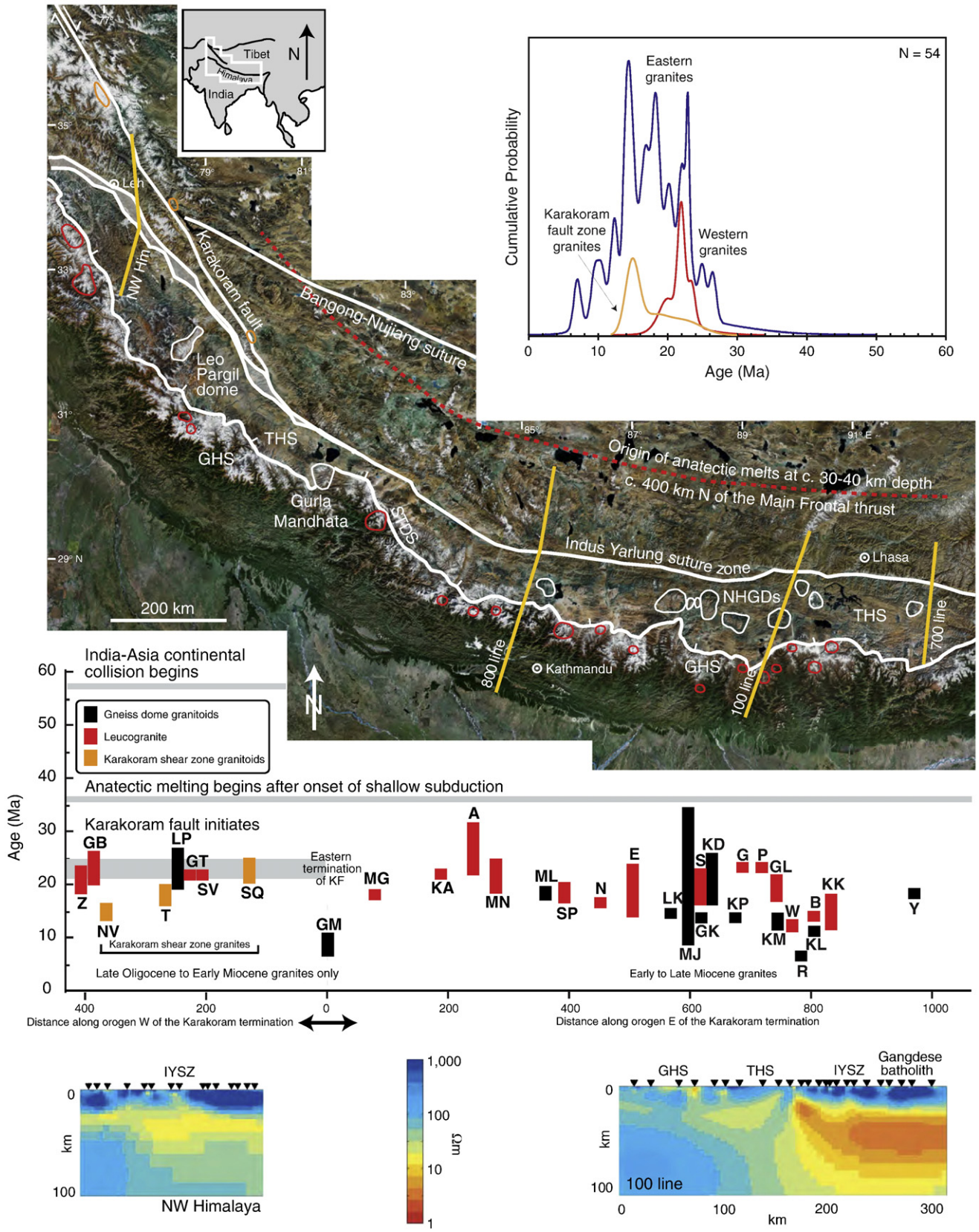

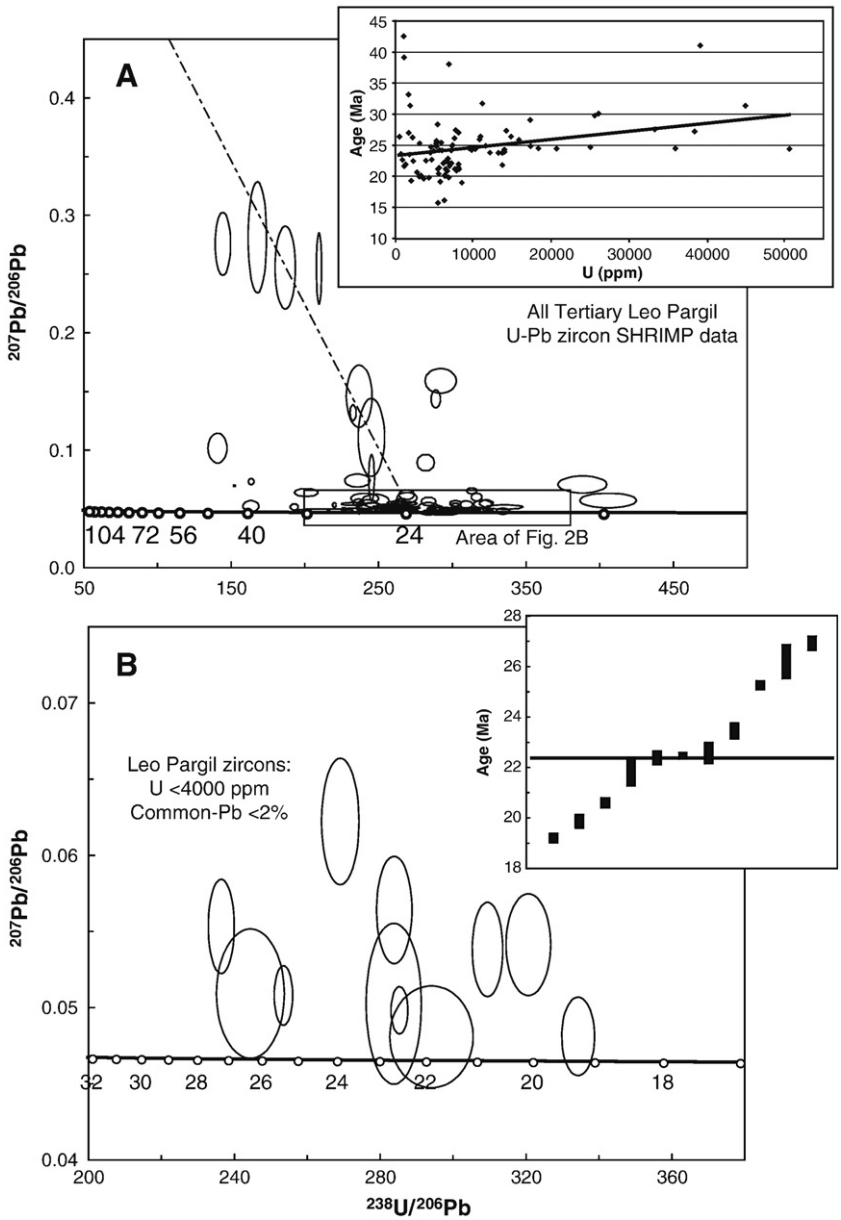

Fig. 2. A: Tera–Wasserburg concordia diagram showing compiled Tertiary U–Pb SHRIMP data for 93 analyses of zircon from eight granitoids from the Leo Pargil gneiss dome, Indian Himalaya (Fig. 1). Data are uncorrected for common Pb; error ellipses are 2σ. Tertiary ages are from zircon domains with high U contents (1000 to >25,000 ppm, see Table 2). Dashed line is a common-Pb mixing line. Inset is an age vs. U concentration scatter plot of data shown in concordia plot A; linear regression of these data shows a trend toward younger ages (c. 24–23 Ma) corresponding to ages from zircon with lower U contents (1000–3000 ppm) and that is consistent with lower intercept ages for individual samples. B: Tera–Wasserburg concordia diagram of a sub-set of thirteen analyses from seven samples shown in Fig. 2A after discordant data (from higher common Pb) and zircons with U concentrations over 4000 ppm are removed. Inset shows a spread of ages from 27 to 19 Ma about a mean of ~22 Ma with no discrete age groups.

southern Tibet that show a divide between a "mantle helium" domain with elevated ^{3}He between the Indus–Yarlung suture and the Bangong–Nujiang suture from a domain of "crustal helium" along the Indus–Yarlung suture (Hoke et al., 2000), and corresponds to the northern extent of highly-conductive middle crust seen in MT data (Unsworth et al., 2005). These geochemical and geophysical constraints show that channel flow melts originate well north of the Karakoram fault in western Tibet (Fig. 1).

Fig. 1. Composite Google Earth image of the Himalaya and southern Tibet showing the Karakoram fault, the Indus–Yarlung suture zone, the South Tibetan Detachment and dated gneiss dome granitoids and Oligo–Miocene leucogranites. Plot shows granite age ranges versus distance along the orogen from the eastern termination of the Karakoram fault (as listed in Table 1) and probability density curves for granite ages (eastern granites: blue; western granites: red; Karakoram fault zone granites: orange). Only Early Miocene granites are found west of the Karakoram fault termination, except for those granites in the Karakoram fault zone; granites east of the Karakoram fault termination span the latest Eocene to Late Miocene. The timing and location of anatectic melting beneath the Tibetan plateau is based on Leech et al. (2005) and Unsworth et al. (2005), respectively; slip initiation on the Karakoram fault is from Valli et al. (2007). The approximate locations of MT profiles in Unsworth et al. (2005) are shown in yellow. Resistivity models derived from inversions of MT data are shown for the NW Himalaya and the 100 line (parallel to the INDEPTH I and II profiles) to demonstrate reduced mid-crustal conductivity in the western Himalaya (from Unsworth et al., 2005); inverted triangles show the locations of the MT stations. White: gneiss domes; Red: leucogranites; Orange: leucogranites in the Karakoram fault zone. Inset map shows the location of the satellite image. A: Annapurna; B: Gophu La; E: Everest–Makalu–Rongbuk; G: Gaowu; GB: Gianbul; GHS: Greater Himalayan sequence; GK: Gomdre–Kouwu; GL: Gasa–Laya; GM: Gurla Mandhata; GT: Gangotri; IYSZ: Indus–Yarlung suture zone; KA: Kalopani; KD: Kuday–Dongong; KK: Kulu Kangri–Gonto La; KL: Karo La–Gyantze; KM: Kangmar; KP: Kampa; LK: Lhagoi Kangri; LP: Leo Pargil; MG: Mugu; MJ: Mabja–Sakya; ML: Malashan–Cuobu; MN: Manaslu; NHGDs: North Himalayan gneiss domes; N: Nyalam; NV: Nubra Valley; P: Paro; R: Renbu; S: Sikkim; SP: Shishapangma–Langtang Lirung; SQ: Shiquanhe; STDS: South Tibetan Detachment System; SV: Shivling; T: Tangste–Pangong Tso; THS: Tethyan Himalayan sequence; W, Wagye La–Masang Kang; Y: Yalashangbo; Z: Zanskar–Gumburanjun. See Table 1 for references.

6. Significance of the Karakoram fault

The ~3 km-wide Karakoram fault zone is a major dextral strike-slip fault system that separates the Indian Himalaya and Ladakh batholith from the Lhasa and Qiangtang terranes of Tibet to the north. Although estimates for the initial timing of slip on the Karakoram fault range between early Miocene and Pliocene time (cf. Review in Valli et al., 2007), recent work by Valli et al. (2007) suggests that the fault has been active since at least 21 Ma. Because this time frame is concurrent with activity on the MCT and STD (e.g., summary in Godin et al., 2006), it raises the prospect that the Karakoram fault could have been involved in conveying crustal melts to shallow crustal levels. Granitoids of the eastern Karakoram terrane are either mid- to Late Cretaceous (Tethyan magmatic arc related to the Ladakh batholith) or

Table 1
Crystallization ages for Late Eocene to Miocene Himalayan granites shown in Fig. 1

Granite body	Abbr.	Age (Ma)	Type	Dating method	Mineral(s)	Reference(s)
Leucogranites in the Greater Himalayan Sequence (listed from west to east as shown in Fig. 1)						
Zanskar–Gumburanjun	Z	24–18	Leucogranite	TIMS/Rb–Sr	Mnz–Zrn–Xtm–Urn–Bt–Ms	Ferrara et al. (1991) (21–18 Ma); Noble and Searle (1995) (21–19 Ma); Dezes et al. (1999) (22 Ma); Walker et al. (1999) (24–21 Ma)
Gianbul	GB	27–20	Gneiss dome	ID–TIMS/SIMS	Mnz	Robyr et al. (2006) (27–20 Ma)
Gangotri	GT	22	Granite	SIMS	Mnz	Harrison et al. (1997) (22 Ma)
Shivling	SV	22	Granite	TIMS	Mnz	Harrison et al. (1997) (22 Ma)
Mugu	MG	18	Granite	TIMS	Mnz	Harrison et al. (1997) (18 Ma)
Kalopani, Nepal	KA	23–22	Leogranite	TIMS	Mnz	Godin et al. (2001) (23–22 Ma)
Annapurna	A	32–22	Leucogranite–migmatite	ID–TIMS	Mnz–Zrn	Hodges et al. (1996) (32–22 Ma)
Manaslu	MN	25–18	Granite	SIMS/TIMS/Rb–Sr	Mnz–Zrn–WR–Kfs–Ms	Deniel et al. (1987) (25 Ma); Copeland et al. (1990) (21–18 Ma); Coleman and Parrish (1995) (19–18 Ma); Harrison et al. (1995) (22 Ma); Harrison et al. (1998), and Harrison et al. (1999) (23–19 Ma)
Shishapangma–Langtang Lirung	SP	20–17	Granite	TIMS	Mnz–Xtm	Parrish and Hodges (1996) (20–18 Ma); Searle et al. (1997) (20–17 Ma)
Nyalam	N	17	Migmatite–granite	TIMS	Mnz	Schärer et al. (1986) (17 Ma)
Everest–Makalu–Rongbuk	E	24–14	Granite	TIMS	Mnz–Xtm	Schärer (1984) (24–21 Ma); Schärer et al. (1986) (14 Ma); Harrison et al. (1995) (22 Ma); Murphy and Harrison (1999) (17–16 Ma); Simpson et al. (2000) (21–20 Ma); Searle et al. (2003) (17 Ma)
Sikkim	S	23–16	Migmatite	MC-ICPMS Sm–Nd	Grt	Harris et al. (2004) (23–16 Ma)
Gaowu	G	23	Leucogranite	TIMS	Mnz	Wu et al. (1998) (23 Ma)
Paro	P	24–23	Leucogranite	TIMS	N/A	R.R. Parrish data, cit. in Searle et al. (2003) (24–23 Ma)
Gasa–Laya, Bhutan	GL	22–17	Leucogranite	SHRIMP	Zrn	R.R. Parrish data, cit. in Searle et al. (2003) (22–17 Ma); Carosi et al. (2006) (20 Ma)
Wagye La–Masang Kang	W	14–12	Leucogranite	TIMS	Mnz	Wu et al. (1998) (12 Ma, Wagye La); R.R. Parrish data, cit. in Searle et al. (2003) (14–13 Ma, Masang Kang)
Gophu La, Bhutan	B	15–14	Granite	Rb–Sr	Ms–Bt	Ferrara et al. (1991) (15–14 Ma)
Khulu Kangri–Gonto La–Eastern Bhutan	KK	18–12	Granite	ID–TIMS	Mnz–Xtm	Edwards and Harrison (1997) (12 Ma); Daniel et al. (2003) (18–13 Ma)
Granitic gneiss domes in the northern Himalaya (from west to east as shown in Fig. 1)						
Leo Pargil	LP	27–19	Gneiss dome	SHRIMP	Zrn	Hassett and Leech (2007) (24–23 Ma); this study
Gurla Mandhata	GM	11–7	Gneiss dome	SIMS	Mnz	Murphy et al. (2002) (11–7 Ma)
Malashan–Cuobu granite	ML	19–18	Gneiss dome	SHRIMP	Zrn	Aoya et al. (2005) (19–18 Ma)
Lhagoi Kangri	LK	15	Granite	TIMS	Mnz	Schärer et al. (1986) (15 Ma); Zhang et al. (2004) (15 Ma)
Mabja–Sakya	MJ	35–9	Gneiss dome	TIMS/SHRIMP	Mnz–Zrn	Schärer et al. (1986) (10–9 Ma); Lee et al. (2006) (23 Ma); Lee and Whitehouse (2007) (35–22 Ma)
Gomdre–Kouwu	GK	14	Granite	TIMS/SHRIMP	Zrn–Mnz	Zhang et al. (2004) (14 Ma); Lee et al. (2006) (14 Ma)
Kuday–Dongong	KD	27–16	Granite	LA–MC–ICPMS	Zrn	Zhang et al. (2004) (27–26 Ma); Lee and Whitehouse (2007) (16 Ma)
Kampa	KP	15–14	Gneiss dome	$^{40}Ar/^{39}Ar$	Bt	Quigley et al. (2006) (15–14 Ma)
Kangmar	KM	15–11	Gneiss dome	$^{40}Ar/^{39}Ar$	Ms–Bt	Lee et al. (2000) (15–11 Ma)
Renbu	R	11–7	Granite	TIMS	Xtm–Zrn	Li et al. (1998) (7 Ma); Hassett and Leech (2008) (11–7 Ma)
Karo La–Gyantze	KL	11–10	Granite	TIMS/SIMS	Mnz–Xtm	Li et al. (1998) (11–10 Ma)
Yalashangbo	Y	18	Gneiss dome	SIMS	Zrn	Aikman et al. (2004) (18 Ma)
Leucogranites in the Karakoram shear zone (from west to east as shown in Fig. 1)						
Nubra Valley	NV	16–14	Granite	ID-TIMS	Zrn	Phillips et al. (2004) (16–14 Ma)
Tangste–Pangong Tso	T	20–14	Granite	SIMS/ID-TIMS	Zrn–Mnz	Searle et al. (1998) (20–16 Ma); Phillips et al. (2004) (16–14 Ma)
Shiquanhe	SQ	25–20	Leucogranite	TIMS/SIMS	Zrn	Lacassin et al. (2004) (25–20 Ma)

Mineral abbreviations: Bt: biotite; Grt: garnet; Kfs: k–feldspar; Mnz: monazite; Ms: muscovite; Urn: uraninite; WR: whole-rock; Xtm: xenotime; Zrn: zircon.

Table 2
Tertiary U–Pb SHRIMP analyses of zircon for Leo Pargil granitoids

Spot	U (ppm)	Th (ppm)	Th/U	Common ^{206}Pb (%)	^{238}U/ ^{206}Pb*	^{207}Pb/^{206}Pb*	^{206}Pb/^{238}U age† (Ma)
01-67-1	5435	28	0.00	0.4	226.5047±0.5028	0.0497±1.9628	28.3±0.1
1-2-11B	6379	103	0.00	1.7	316.4695±0.7448	0.0601±3.4944	20.0±0.2
1-2-9B	8203	86	0.02	1.0	302.1465±0.7794	0.0547±2.9250	21.1±0.2
1-2-7B	4953	60	0.00	1.2	264.2882±0.8188	0.0559±3.0320	24.1±0.2
1-2-3B	6029	102	0.01	0.2	266.2271±0.5355	0.0485±1.8292	24.1±0.1
1-2-5B	50605	1153	0.02	0.2	263.6364±0.2950	0.0484±1.1715	24.3±0.1
1-2-13B	35947	486	0.01	0.1	263.2693±0.2335	0.0472±0.9375	24.4±0.1
1-2-14B	25032	271	0.01	0.2	260.6944±0.3074	0.0483±1.0573	24.6±0.1
1-2-4B	4574	42	0.01	10.8	232.6482±0.5725	0.1320±3.3489	24.7±0.2
1-2-10B	7364	84	0.02	0.5	256.4542±0.7008	0.0506±2.8801	25.0±0.2
1-2-2B	15884	128	0.01	0.2	248.7131±0.3252	0.0482±1.2821	25.8±0.1
1-2-8B	38405	440	0.00	0.0	236.7787±0.2873	0.0468±1.1426	27.2±0.1
1-2-1B	33298	1364	0.02	0.0	234.0059±0.1980	0.0468±0.7890	27.5±0.1
1-2-12B	44948	1039	0.00	0.1	205.4415±2.6008	0.0471±0.8826	31.3±0.8
1-2-6B	39152	4355	0.00	2.9	152.1733±0.2383	0.0697±0.6785	41.0±0.1
1-2-1	2052	19	0.00	0.2	334.3019±0.8893	0.0481±3.5322	19.2±0.2
1-2-6	3661	71	0.01	12.3	288.8032±0.7189	0.1437±3.4625	19.5±0.2
1-2-5	5624	55	0.00	0.1	302.0240±0.4950	0.0473±1.9385	21.3±0.1
1-2-8	6159	88	0.00	0.0	291.9944±0.5670	0.0469±1.9385	22.0±0.1
1-2-4	6760	103	0.00	0.1	282.2483±0.4853	0.0473±1.9364	22.8±0.1
1-2-2	9473	186	0.01	1.0	260.7024±0.4447	0.0542±2.4145	24.4±0.1
1-2-7	25603	379	0.00	0.3	216.0270±0.2012	0.0489±0.7040	29.7±0.1
8-17-13	546	1	0.00	0.9	242.5202±1.9905	0.0535±5.2678	26.3±0.5
8-17-19	1701	3	0.00	0.6	192.8161±0.8833	0.0518±3.2890	33.1±0.3
8-17-6	1144	2	0.00	0.7	163.3496±2.1646	0.0524±5.8664	39.1±0.9
28-50-5	2303	6	0.01	1.2	283.8478±1.1224	0.0564±4.1196	22.4±0.3
28-50-8	1830	4	0.00	2.0	269.0436±1.2581	0.0622±4.3914	23.4±0.3
28-50-12	1717	6	0.01	1.1	236.4040±0.9894	0.0553±3.6981	26.9±0.3
28-50-13	1084	6	0.01	6.9	140.7177±3.0010	0.1018±8.2028	42.5±1.4
27-49-10	3310	16	0.01	2.4	313.1985±0.7119	0.0655±2.4659	20.1±0.1
27-49-8	6351	17	0.01	0.3	318.5449±0.5602	0.0488±2.2123	20.1±0.1
27-49-15	6672	19	0.02	0.2	308.9485±0.5425	0.0483±1.8982	20.8±0.1
27-49-23	6479	16	0.00	0.2	304.0796±0.4821	0.0481±1.9159	21.1±0.1
27-49-21	8112	31	0.01	0.1	300.8374±0.4084	0.0476±1.6390	21.4±0.1
27-49-3	6964	14	0.01	0.1	298.0566±0.5810	0.0477±1.9788	21.6±0.1
27-49-19	13733	49	0.01	0.1	295.5560±0.3566	0.0475±1.2428	21.7±0.1
27-49-11	8132	26	0.02	0.4	293.2493±0.4663	0.0496±1.8180	21.9±0.1
27-49-5	735	11	0.00	1.6	269.1235±1.6527	0.0595±5.1157	23.5±0.4
27-49-16	13738	38	0.02	0.4	270.5072±0.9646	0.0495±1.4460	23.7±0.2
27-49-17	13242	40	0.00	0.1	271.1500±0.3156	0.0474±1.2620	23.7±0.1
27-49-22	14000	42	0.00	0.5	264.3846±0.5231	0.0503±1.7315	24.2±0.1
27-49-12	10280	34	0.01	0.2	263.6820±0.3819	0.0480±1.5094	24.4±0.1
27-49-18	20708	84	0.01	0.1	263.3894±0.2582	0.0475±1.0266	24.4±0.1
27-49-1	11587	52	0.01	0.8	256.9371±0.4185	0.0526±2.0069	24.8±0.1
27-49-6	10817	50	0.01	0.6	247.1503±0.3980	0.0512±1.2914	25.9±0.1
27-49-4	26097	154	0.02	0.3	213.6800±5.7401	0.0487±2.0733	30.0±1.7
26-45-26	4324	26	0.01	1.0	323.1784±0.9387	0.0548±3.5530	19.7±0.2
26-45-17	6876	73	0.00	0.3	325.1662±0.5009	0.0485±1.8829	19.7±0.2
26-45-11	3060	23	0.01	1.0	320.6458±1.2579	0.0541±4.0675	19.9±0.3
26-45-10	2812	11	0.00	0.9	309.4394±0.8916	0.0538±3.7895	20.6±0.2
26-45-28	5487	14	0.01	0.8	302.2419±0.5315	0.0532±2.0061	21.1±0.1
26-45-8	1144	5	0.02	5.4	281.9503±1.3719	0.0895±5.1441	21.6±0.3
26-45-1	7132	63	0.00	0. 1	292.7905±0.4675	0.0470±1.8887	22.0±0.1
26-45-23	7219	57	0.00	0.6	290.5177±0.6495	0.0510±2.5084	22.0±0.1
26-45-30	6721	81	0.01	0.6	286.8399±0.4735	0.0513±1.8280	22.3±0.1
26-45-20	6482	128	0.02	0.5	286.2582±0.5044	0.0502±1.9544	22.4±0.1
26-45-16	3949	29	0.01	0.4	285.2835±0.5284	0.0498±2.0482	22.5±0.1
26-45-24	934	6	0.01	0.5	283.7278±1.7694	0.0503±6.9313	22.6±0.4
26-45-27	4670	65	0.01	26.3	209.5843±0.5396	0.2548±7.9130	22.6±0.8
26-45-15	12155	75	0.01	1.0	268.3540±1.8495	0.0547±1.7948	23.7±0.4
26-45-32	9787	101	0.02	0.7	264.3687±0.3748	0.0518±3.1917	24.2±0.1
26-45-33	7309	63	0.01	1.1	262.5130±1.6597	0.0553±1.4844	24.2±0.4
26-45-31	17367	294	0.00	0.6	258.0696±0.3019	0.0512±1.1614	24.8±0.1
26-45-6	7289	41	0.01	0.5	257.7678±0.5158	0.0506±2.5163	24.8±0.1
26-45-29	3122	56	0.01	0.5	253.4620±0.6517	0.0508±2.5363	25.2±0.2
26-45-18	5262	37	0.02	3.8	245.2524±0.5236	0.0766±16.9779	25.2±0.5
26-45-22	17309	157	0.01	0.9	219.9619±0.3430	0.0534±2.3517	29.0±0.1
26-45-19	6890	212	0.01	3.4	163.5843±0.7100	0.0734±2.2952	38.0±0.3
63-02	2216	11	0.01	1.8	244.4043±2.515	0.0509±5.5013	26.2±0.7
63-05	1931	29	0.00	9.3	200.8749±2.5719	0.0640±3.4285	31.3±0.8
50-2	14867	134	0.00	2.1	240.5942±2.5689	0.0590±4.8283	26.3±0.7
50-3	7191	50	0.01	8.0	245.0704± ±2.4075	0.1110±19.7434	24.1±0.9
50-4	10931	74	0.00	5.9	235.6578±2.3807	0.0742±4.9655	26.3±0.6

(continued on next page)

Table 2 (*continued*)

Spot	U (ppm)	Th (ppm)	Th/U	Common ^{206}Pb (%)	^{238}U/ ^{206}Pb*	^{207}Pb/^{206}Pb*	^{206}Pb/^{238}U age† (Ma)
50-6	5288	57	0.01	8.6	247.7437±2.4190	0.0569±6.6352	25.6±0.6
50-7	5923	30	0.01	33.8	186.6903±2.4079	0.2555±9.1031	25.4±1.3
50-8	7601	26	0.00	0.6	245.9362±2.4005	0.0493±1.6178	26.1±0.6
50-9	14258	165	0.01	0.8	233.3635±2.3852	0.0543±1.3589	27.3±0.7
50-10	11179	45	0.01	27.0	144.2910±2.4012	0.2757±6.3931	31.7±1.5
50-11	7839	24	0.01	0.5	307.5100±2.4373	0.0490±1.8048	20.9±0.5
50-12	5682	23	0.01	1.2	265.3596±2.4238	0.0490±2.3878	24.2±0.6
50-13	14014	101	0.04	1.3	268.1815±2.3925	0.0512±1.4160	23.9±0.6
50-14	18358	148	0.01	0.7	261.6922±2.3778	0.0508±1.1344	24.5±0.6
50-16	8554	129	0.01	16.0	292.0832±2.3929	0.1591±4.3464	18.9±0.5
50-17	7644	23	0.02	0.3	303.6581±2.4121	0.0496±1.7895	21.1±0.5
50-19	8129	55	0.01	29.0	167.7782±2.4497	0.2812±11.0463	27.0±1.8
50-20	5579	129	0.02	1.4	315.3477±2.4286	0.0495±2.5028	20.3±0.5
50-21	6319	27	0.02	3.7	388.3311±2.8018	0.0709±6.7376	16.1±0.5
50-22	7739	55	0.00	0.9	234.1992±2.4141	0.0492±2.2651	27.4±0.7
50-32	5784	22	0.00	2.3	335.3812±2.4227	0.0517±2.3330	19.1±0.5
50-23	5290	59	0.03	1.6	258.0614±2.4093	0.0525±1.9998	24.7±0.6
50-26	5474	16	0.00	19.0	405.7337±3.1158	0.0573±7.1046	15.6±0.5
50-27	4509	37	0.11	12.6	236.8208±2.4429	0.1460±11.9469	23.8±0.9
50-28	1344	10	0.01	1.5	294.0466±2.5689	0.0481±4.5818	21.8±0.6

Note: 1σ error unless noted otherwise.
*Uncorrected; error given as percentage.
†Corrected for ^{207}Pb.

Miocene (Le Fort, 1988; Phillips et al., 2004; Phillips, 2008). Miocene leucogranites in the Karakoram fault zone are variably deformed and have been interpreted as pre- and syn-deformation on the fault (Weinberg et al., 2000; Valli et al. 2007); the presence of leucogranites in the Karakoram fault zone may be explained by synchronous deformation, metamorphism and plutonism (e.g., Solar et al., 1998; Schneider et al., 1999; Weinberg et al., 2004) or melts generated by shear heating (e.g., Nabelek et al., 2001), though here I propose that the leucogranites are derived from anatectic partial melts in a mid-crustal ductile channel.

If the Karakoram fault has affected channel flow in the western Himalaya, the timing slip began on the fault must be established. Slip initiation on the Karakoram fault is dated from syn-kinematic granites in the shear zone in the Shiquanhe region at c. 25–21 Ma (Valli et al., 2007). ^{40}Ar/^{39}Ar and apatite (U–Th)/He thermochronology results from the same area show cooling between 21 and 4 Ma demonstrating that the Karakoram fault was active throughout the Miocene and motion continued at least until the Early Pliocene (Valli et al., 2007). Granites and mylonitic leucogranites from the Tangste–Pangong and Nubra Valley sections of the Karakoram fault yield U–Pb ages for zircon of ~18 Ma (Searle et al., 1998) and ~16 Ma (Phillips et al., 2004) interpreted as dating crystallization; ages for cross-cutting dikes in these locations are suggested to bracket the initiation of fault motion to between 16 and 14 Ma (Phillips et al., 2004) but evidence that the Tangste granite is actually synkinematic with the Karakoram fault suggests that the 18–16 Ma dates are lower limits for the timing of slip initiation (Valli et al., 2007). So the Karakoram fault was active by the Early Miocene and slip continued throughout the Miocene and Early Pliocene when channel flow was ongoing.

Geophysical evidence suggests that the Karakoram fault is a crustal-scale fault that should intersect the partial melts in the mid-crustal channel at 30–40 km; a change in the nature of the receiver functions from south to north across the fault suggests a significant difference in the crustal structure across the fault at the depth of the Moho (Rai et al., 2006). Ductile shear zones commonly act as fluid pathways into the middle crust (Read and Cartwright, 2000; Clark et al., 2005); linear alignments and spatial associations of granites in the Periadriatic fault system in the Alps and part of the South Armorican shear zone in the French Central Massif demonstrate that strike-slip shear zones can act as an ascent pathway for magmas from 15–40 km depth (Rosenberg, 2004; Gébelin et al., 2006). Further, Evans et al. (1997) show that upper crustal brittle fault zones not only enhance fluid flow parallel to a fault plane, but restrict fluid flow across a fault. Late Oligocene to Middle Miocene (25–14 Ma) leucogranites are found in three locations along the Karakoram fault (the Nubra Valley, Tangste–Pangong, and Shiquanhe areas, Fig. 1; Searle et al., 1998; Lacassin et al., 2004; Phillips et al., 2004), located between the source region for channel melts beneath the Tibetan plateau and the granite gneiss domes and leucogranite bodies south of the suture zone (Fig. 1). When slip began on the Karakoram fault in the latest Oligocene–Early Miocene, it may have acted as a barrier to southward flow of granites in the channel and acted as a vertical conduit for magmas within the shear/fault zone.

7. Discussion

If the Karakoram fault acted as a barrier to the flow of granitoid melts in a mid-crustal channel, the channel should have been melt-starved south of the Karakoram fault in the west and more abundant and younger granites should be expected in the GHS and granitic gneiss domes east of the Karakoram fault termination as the channel continued to flow south after c. 21 Ma. This prediction is correct: granite bodies are significantly more abundant east of the Karakoram fault termination; this can be seen in the field, on satellite imagery (gneiss domes appear in Fig. 1 as light-colored granites rimmed by green metamorphic mantles), and in the number of dated granitoid bodies shown in Table 1. It is reasonable to use the number of dated granite bodies as a proxy for actual abundance because of the accessibility to most of the areas in southern Tibet and northern India, and because additional undated domes are present in the eastern Himalaya (but not the west) as seen on satellite imagery (Fig. 1). In the eastern Himalaya, there are abundant leucogranites from 25–12 Ma with the youngest granites dated at ~7 Ma from the Renbu dome (Fig. 1); in the western Himalaya, leucogranites are restricted to the Early Miocene. This model also predicts that granitoids would leak up the Karakoram fault similar to the lines of granites in the Periadriatic fault system (Rosenberg, 2004); this prediction is satisfied by 25–14 Ma leucogranites in three locations along the Karakoram fault (Fig. 1). If the Karakoram fault is indeed a barrier to horizontal ductile flow and facilitates vertical melt migration, then future tectonic

models for the Himalaya should recognize the differences between the western and eastern segments of the orogen starting in the Miocene, rather than emphasizing along-strike uniformity.

The much smaller melt percentage (2–4%) inferred from MT profiling and a lack of a continuous low-velocity mid-crustal layer in the NW Himalaya south of the Karakoram fault indicates insufficient melt for ductile flow and may represent a lack of melt supply (Gaillard et al., 2004; Rosenberg and Handy, 2005; Unsworth et al., 2005; Oreshin et al., 2008). The modern configuration of mid-crustal conductivity has likely existed since the Early Miocene when channel flow may have shut down in the western Himalaya c. 25–21 Ma. Partial melts have continued to be intruded into the upper crust during the Quaternary based on locally variable high modern heat flow (Gupta et al., 1983; Jaupart et al., 1985) and seismic bright spots from small volume partial melts (Makovsky and Klemperer, 1999). Channel flow is likely still active in the eastern Himalaya where it may be a tunneling channel flow similar to the models for the growth of the Tibetan plateau via mid-crustal extrusion (Beaumont et al., 2006; Hodges, 2006; Klemperer, 2006).

Acknowledgments

I thank Joe Wooden, Frank Mazdab, and Willie Hassett for help with SHRIMP sample preparation, data analysis and reduction; Rasmus Thiede for generously providing some zircon separates for U–Pb geochronology; and Sandeep Singh and Kristen Cook for assistance in the field. This work was supported by funding from San Francisco State University and the National Science Foundation. Many thanks to Djordje Grujic and one anonymous reviewer for very helpful reviews; an earlier version of this manuscript was improved based on reviews by Roberto Weinberg, Aaron Yoshinobu, and one anonymous reviewer.

References

Aikman, A.B., Harrison, T.M., Lin, D., 2004. Preliminary results from the Yala–Xiangbo leucogranite dome, SE Tibet. 19th Himalaya–Karakoram–Tibet workshop extended abstracts, Niseko, Japan, p. 91.

Aoya, M., Wallis, S.R., Terada, K., Lee, J., Kawakami, T., Wang, Y., Heizler, M., 2005. North–south extension in the Tibetan crust triggered by granite emplacement. Geology 33, 853–856.

Beaumont, C., Jamieson, R.A., Nguyen, M.H., Medvedev, S., 2004. Crustal channel flows: 1. Numerical models with applications to the tectonics of the Himalayan–Tibetan orogen. J. Geophys. Res. 109. doi:10.1029/2003JB002809.

Beaumont, C., Nguyen, M., Jamieson, R., Ellis, S., 2006. Crustal flow modes in large hot orogens,. In: Law, R.D., Searle, M.P., Godin, L. (Eds.), Channel Flow, Ductile Extrusion and Exhumation in Continental Collision Zones. Geol. Soc., London, Spec. Pub., vol. 268, pp. 91–145.

Bendick, R., Flesch, L., 2007. Reconciling lithospheric deformation and lower crustal flow beneath central Tibet. Geology 35, 895–898.

Black, L.P., Kamo, S.L., Allen, C.M., Davis, D.W., Aleinikoff, J.N., Valley, J.W., Mundil, R., Campbell, I.H., Korsch, R.J., Williams, I.S., Foudoulis, C., 2004. Improved $^{206}Pb/^{238}U$ microprobe geochronology by the monitoring of a trace-element-related matrix effect: SHRIMP ID-TIMS, ELA-ICP-MS, and oxygen isotope documentation for a series of zircon standards. Chem. Geol. 205, 115–140.

Carosi, R., Montomoli, C., Rubatto, D., Visona, D., 2006. Normal-sense shear zones in the core of the Higher Himalayan crystallines (Bhutan Himalaya): evidence for extrusion? In: Law, R.D., Searle, M.P., Godin, L. (Eds.), Channel Flow, Ductile Extrusion and Exhumation in Continental Collision Zones. Geol. Soc., London, Spec. Pub., vol. 268, pp. 425–444.

Chen, L., Booker, J., Jones, A., Nong, W., Unsworth, M., Wei, W., Tan, H., 1996. Electromagnetic images of colliding continents: a magnetotelluric survey of the Tsangpo suture zone and surrounding regions. Science 274, 1694–1696.

Clark, C., Schmidt Mumm, A., Faure, K., 2005. Timing and nature of fluid flow and alteration during Mesoproterozoic shear zone formation, Olary Domain, South Australia. J. Metam. Geol. 23, 147–164.

Coleman, M.E., Parrish, R.R., 1995. Constraints on Miocene high-temperature deformation and anatexis within the greater Hiimalaya from U–Pb geochronology. Eos Trans., Am. Geophys. Union 76, F708.

Copeland, P., Harrison, T.M., Le Fort, P., 1990. Age and cooling history of the Manaslu granite: implications for Himalayan tectonics. J. Volcanol. Geotherm. Res. 44, 33–50.

Daniel, C.G., Hollister, L.S., Parrish, R.R., Grujic, D., 2003. Exhumation of the main central thrust from lower crustal depths, eastern Bhutan Himalaya. J. Metam. Geol. 21, 317–334.

DeCelles, P.G., Robinson, D.M., Zandt, G., 2002. Implications of shortening in the Himalayan fold-and-thrust belt for uplift of the Tibetan plateau. Tectonics 21. doi:10.1029/2001TC001322.

Deniel, C., Vidal, P., Fernandez, A., Le Fort, P., Peucat, J.-J., 1987. Isotopic study of the Manaslu granite (Himalaya, Nepal): inferences on the age and source of Himalayan leucogranites. Contrib. Mineral. Petrol. 96, 78–92.

Dezes, P.J., Vannay, J.-C., Steck, A., Bussy, F., Cosca, M., 1999. Synorogenic extension: quantitative constraints on the age and displacement of the Zanskar shear zone (northwest Himalaya). Geol. Soc. Am. Bull. 111, 364–374.

Edwards, M.A., Harrison, T.M., 1997. When did the roof collapse? Late Miocene north–south extension in the high Himalaya revealed by Th–Pb monazite dating of the Khula Kangri granite. Geology 25, 543–546.

Evans, J.P., Forster, C.B., Goddard, J.V., 1997. Permeability of fault-related rocks, and implications for hydraulic structure of fault zones. J. Struct. Geol. 19, 1393–1404.

Ferrara, G., Lombardo, B., Tonarini, S., Turi, B., 1991. Sr, Nd and O isotopic characterization of the Gophu La and Gumburanjun leucogranites (High Himalaya). Schweiz. Mineral. Petrogr. Mitt. 71, 35–51.

Francheteau, J., Jaupart, C., Shen, X.J., Kang, W.H., Lee, D.L., Bai, J.C., Wei, H.P., Deng, H.Y., 1984. High heat flow in southern Tibet. Nature 307, 32–36.

Gaillard, F., Scaillet, B., Pichavant, M., 2004. Evidence for present-day leucogranite pluton growth in Tibet. Geology 32, 801–804. doi:10.1130/G20577.1.

Gébelin, A., Martelet, G., Chen, Y., Brunel, M., Faure, M., 2006. Structure of late Variscan Millevaches leucogranite massif in the French Massif Central: AMS and gravity modeling results. J. Struct. Geol. 28, 148–169.

Godin, L., Parrish, R.R., Brown, R.L., Hodges, K.V., 2001. Crustal thickening leading to exhumation of the Himalayan metamorphic core of central Nepal: insight from U–Pb geochronology and $^{40}Ar/^{39}Ar$ thermochronology. Tectonics 20, 729–747.

Godin, L., Grujic, D., Searle, M.P., Law, R.D., 2006. Channel flow, extrusion, and exhumation in continental collision zones: an introduction. In: Law, R.D., Searle, M.P., Godin, L. (Eds.), Channel Flow, Ductile Extrusion and Exhumation in Continental Collision Zones. Geol. Soc., London, Spec. Pub., vol. 268, pp. 1–23.

Grujic, D., 2006. Channel flow and continental collision tectonics: an overview. In: Law, R.D., Searle, M.P., Godin, L. (Eds.), Channel Flow, Ductile Extrusion and Exhumation in Continental Collision Zones. Geol. Soc., London, Spec. Pub., vol. 268, pp. 25–37.

Grujic, D., Casey, M., Davidson, C., Hollister, L.S., Kündig, R., Pavlis, T., Schmid, S., 1996. Ductile extrusion of the Higher Himalayan crystalline in Bhutan: evidence from quartz microfabrics. Tectonophys. 260, 21–43.

Grujic, D., Hollister, L., Parrish, R.R., 2002. Himalayan metamorphic sequence as an orogenic channel: insight from Bhutan. Earth Planet. Sci. Lett. 198, 177–191.

Gupta, M.L., Sharma, S.R., Drolia, R.K., Singh, S., 1983. Subsurface thermal conditions of Puga Valley hydrothermal field, Himalaya, India. J. Geophys. 54, 51–59.

Harris, N.B.W., Caddick, M., Kosler, J., Goswami, S., Vance, D., Tindle, A.G., 2004. The pressure–temperature–time path of migmatites from the Sikkim Himalaya. J. Metam. Geol. 22, 249–264.

Harrison, T.M., McKeegan, K.D., LeFort, P., 1995. Detection of inherited monazite in the Manaslu leucogranite by $^{208}Pb/^{232}Th$ ion microprobe dating: crystallization age and tectonic significance. Earth Planet. Sci. Lett. 133, 271–282.

Harrison, T.M., Lovera, O.M., Grove, M., 1997. New insights into the origin of two contrasting Himalayan granite belts. Geology 25, 899–902.

Harrison, T.M., Grove, M., Lovera, O.M., Catlos, E.J., 1998. A model for the origin of Himalayan anatexis and iinverted metamorphism. J. Geophys. Res. 103, 27,017–27,032.

Harrison, T.M., Grove, M., McKeegan, K.D., Coath, C.D., Lovera, O.M., Le Fort, P., 1999. Origin and episodic emplacement of the Manaslu Intrusive Complex, central Himalaya. J. Petrol. 40, 3–19.

Hassett, W., Leech, M.L., 2007. Early Miocene granitoids from the Leo Pargil gneiss domes, northwest Himalaya. Eos Trans., Am. Geophys. Union 88 Fall Meeting Supp., Abstract T31D-0668.

Hassett, W., Leech, M.L., 2008. U–Pb and trace element data from the Renbu gneiss dome, southeast Tibet. Eos Trans., Am. Geophys. Union 88 Fall Meeting Supp., Abstract T33B-2049.

Hodges, K.V., 2006. A synthesis of the channel flow-extrusion hypothesis as developed for the Himalayan–Tibetan orogenic system. In: Law, R.D., Searle, M.P., Godin, L. (Eds.), Channel Flow, Ductile Extrusion and Exhumation in Continental Collision Zones. Geol. Soc., London, Spec. Pub., vol. 268, pp. 71–90.

Hodges, K.V., Parrish, R.R., Searle, M.P., 1996. Tectonic evolution of the central Annapurna Range, Nepalese Himalaya. Tectonics 15, 1264–1291.

Hodges, K.V., Hurtado, J.M., Whipple, K.X., 2001. Southward extrusion of Tibetan crust and its effect on Himalayan tectonics. Tectonics 20, 799–809.

Hoke, L., Lamb, S., Hilton, D.R., Poreda, R.J., 2000. Southern limit of mantle-derived geothermal helium emissions in Tibet: implications for lithospheric structure. Earth Planet. Sci. Lett. 180, 297–308.

Jamieson, R.A., Beaumont, C., Medvedev, S., Nguyen, M.H., 2004. Crustal channel flows: 2. Numerical models with implications for metamorphism in the Himalayan–Tibetan orogen. Geophys. Res 109, B06407. doi:10.1029/2003JB002811.

Jaupart, C., Francheteau, J., Shen, X.-J., 1985. On the thermal structure of the southern Tibetan crust. Geophys. J. Royal Astronom. Soc. 81, 131–155.

Kind, R., Yuan, X., Saul, J., Nelson, D., Sobolev, S.V., Mechie, J., Zhao, W., Kosarev, G., Ni, J., Achauer, U., Jiang, M., 2002. Seismic images of crust and upper mantle beneath Tibet; evidence for Eurasian Plate subduction. Science 298, 1219–1221.

King, J., Harris, N., Argles, T., Parrish, R., Charlier, B., Sherlock, S., Zhang, H.F., 2007. First field evidence of southward ductile flow of Asian crust beneath southern Tibet. Geology 35, 727–730.

Klemperer, S.L., 2006. Crustal flow in Tibet: geophysical evidence for the physical state of Tibetan lithosphere, and inferred patterns of active flow. In: Law, R.D., Searle, M.P., Godin, L. (Eds.), Channel Flow, Ductile Extrusion and Exhumation in Continental Collision Zones. Geol. Soc., London, Spec. Pub., vol. 268, pp. 39–70.

Klemperer, S.L., 2008. Reconciling lithospheric deformation and lower crustal flow beneath central Tibet. Comment, Geology. doi:10.1130/G25097C.1.

Lacassin, R., Valli, R., Arnaud, N., Leloup, P.H., Paquette, J.L., Haibing, L., Tapponnier, P., Chevalier, M.-L., Guillot, S., Maheo, G., Zhiqin, X., 2004. Large-scale geometry, offset and kinematic evolution of the Karakorum fault, Tibet. Earth Planet. Sci. Lett. 219, 255–269.

Lee, J., Whitehouse, M.J., 2007. Onset of mid-crustal extensional flow in southern Tibet: Evidence from U–Pb zircon ages. Geology 35, 45–48.

Lee, J., Hacker, B.R., Dinklage, W.S., Wang, Y., Gans, P., Calvert, A., Wan, J., Chen, W., Blythe, A.E., McClelland, W., 2000. Evolution of the Kangmar dome, southern Tibet: structural, petrologic, and thermochronologic constraints. Tectonics 19, 872–895.

Lee, J., McClelland, W., Wang, Y., Blythe, A., McWilliams, M., 2006. Oligocene–Miocene middle rustal flow in southern Tibet: geochronology of Mabja Dome, in. In: Law, R.D., Searle, M.P., Godin, L. (Eds.), Channel Flow, Ductile Extrusion and Exhumation in Continental Collision Zones. Geol. Soc., London, Spec. Pub., vol. 268, pp. 445–469.

Leech, M.L., Singh, S., Jain, A.K., Klemperer, S.L., Manickavasagam, R.M., 2005. The onset of India–Asia continental collision: early, steep subduction required by the timing of UHP metamorphism in the western Himalaya. Earth Planet. Sci. Lett. 234, 83–97.

Le Fort, P., 1988. Granites in the tectonic evolution of the Himalaya, Karakoram and southern Tibet. Philos. Trans. Roy. Soc. London, Series A 326, 281–299.

Li, J., Miller, B.V., Nelson, K.D., Samson, S.D., 1998. Two belts of collisional granite in the Himalaya? Eos Trans., Am. Geophys. Union T52A-06.

Ludwig, K.R., 1999. Using Isoplot/Ex, Version 2.01: A Geochronological Toolkit for Microsoft Excel. Spec. Pub., vol. 1a. Berkeley Geochronology Center, Berkeley, CA. 47 pp.

Ludwig, K.R., 2001. Eliminating mass-fractionation effects on U–Pb isochron ages without double-spiking of Pb. Geochim. Cosmochim. Acta 65, 3139–3145. doi:10.1016/S0016-7037(01)00637-8.

Makovsky, Y., Klemperer, S.L., 1999. Measuring the seismic properties of Tibetan bright spots: evidence for free aqueous fluids in the Tibetan middle crust. J. Geophys. Res. 104, 10,795–10,825.

Medvedev, S., Beaumont, C., 2006. Growth of continental plateaus by channel injection: models designed to address constraints and thermomechanical consistency. In: Law, R.D., Searle, M.P., Godin, L. (Eds.), Channel Flow, Ductile Extrusion and Exhumation in Continental Collision Zones. Geol. Soc., London, Spec. Pub., vol. 268, pp. 147–164.

Murphy, M.A., Harrison, T.M., 1999. Relationship between leucogranites and the Qomolangma detachment in the Rongbuk valley, south Tibet. Geology 27, 831–834.

Murphy, M.A., Yin, A., Kapp, P., Harrison, T.M., Manning, C.E., Ryerson, F.J., Lin, D., Jinghui, G., 2002. Structural evolution of the Gurla Mandhata detachment system, southwest Tibet: implications for the eastward extent of the Karakoram fault system. Geol. Soc. Am. Bull. 114, 428–447.

Nabelek, P.I., Liu, M., Sirbescu, M.-L., 2001. Thermo-rheological, shear heating model for leucogranite generation, metamorphism, and deformation during the Proterozoic Trans-Hudson orogeny, Black Hills, South Dakota. Tectonophysics 342, 371–388.

Nelson, K.D., Zhao, W., Brown, L.D., Kuo, J., Che, J., Liu, X., Klemperer, S.L., Makovsky, Y., Meissner, R., Mechie, J., Kind, R., Wenzel, F., Ni, J., Nabelek, J., Leshuo, C., Tan, H., Wei, W., Jones, A.G., Booker, J., Unsworth, M., Kidd, W.S.F., Hauck, M., Alsdorf, D., Ross, A., Cogan, M., Wu, C., Sandvol, E., Edwards, M., 1996. Partially molten middle crust beneath southern Tibet: synthesis of Project INDEPTH results. Science 274, 1684–1688.

Noble, S.R., Searle, M.P., 1995. Age of crustal melting and leucogranite formation from U–Pb zircon and monazite dating in the western Himalaya, Zanskar, India. Geology 23, 1135–1138.

Oreshin, S., Kiselev, S., Vinnik, L., Prakasam, K.S., Rai, S.S., Makeyeva, L., Savvin, Y., 2008. Crust and mantle beneath western Himalaya, Ladakh and western Tibet from integrated seismic data. Earth Planet. Sci. Lett. 271, 75–87.

Parrish, R.R., Hodges, K.V., 1996. Isotopic constraints on the age and provenance of the Lesser and Greater Himalayan sequences. Geol. Soc. Am. Bull. 108, 904–911.

Phillips, R.J., 2008. Geological map of the Karakoram fault zone, eastern Karakoram, Ladakh, NW Himalaya. J. Maps 2008, 21–37.

Phillips, R.J., Parrish, R.R., Searle, M.P., 2004. Age constraints on ductile deformation and long-term slip rates along the Karakoram fault zone, Ladakh. Earth Planet. Sci. Lett. 226, 305–319.

Quigley, M., Liangjun, Y., Xiaohan, L., Wilson, C.J.L., Sandiford, M., Phillips, D., 2006. $^{40}Ar/^{39}Ar$ thermochronology of the Kampa dome, southern Tibet: implications for tectonic evolution of the North Himalayan gneiss domes. Tectonophysics 421, 269–297.

Rai, S.S., Priestley, K., Gaur, V.K., Mitra, S., Singh, M.P., Searle, M., 2006. Configuration of the Indian Moho beneath the NW Himalaya and Ladakh. Geophys. Res. Lett. 33. doi:10.1029/2006GL026076.

Read, C.M., Cartwright, I., 2000. Meteoric fluid infiltration in the middle crust during shearing: examples from the Arunta Inlier, central Australia. J. Geochem. Explor. 69–70, 333–337.

Robyr, M., Hacker, B.R., Mattinson, J.M., 2006. Doming in compressional orogenic settings: new geochronological constraints from the NW Himalaya. Tectonics 25. doi:10.1029/2004TC001774.

Rosenberg, C.L., 2004. Shear zones and magma ascent: a model based on a review of the Tertiary magmatism in the Alps. Tectonics 23. doi:10.1029/2003TC001526.

Rosenberg, C.L., Handy, M.R., 2005. Experimental deformation of partially melted granite revisited: implications for the continental crust. J. Metam. Geol. 23, 19–28.

Schärer, U., 1984. The effect of initial ^{230}Th disequilibration of U–Pb ages: the Makalu case. Earth Planet. Sci. Lett. 67, 191–204.

Schärer, U., Xu, R., Allegre, C.J., 1986. U–(Th)–Pb systematics and ages of Himalayan leucogranites, south Tibet. Earth Planet. Sci. Lett. 77, 35–48.

Schneider, D.A., Edwards, M.A., Kidd, W.S.F., Zeitler, P.K., Coath, C.D., 1999. Early Miocene anatexis identified in the western syntaxis, Pakistan Himalaya. Earth Planet. Sci. Lett. 167, 121–129.

Searle, M.P., Parrish, R.R., Hodges, K.V., Hurford, A., Ayres, M.W., Whitehouse, M.J., 1997. Shisha Pangma leucogranite, south Tibetan Himalaya: field relations, geochemistry, age, origin and emplacement. J. Geol. 105, 295–317.

Searle, M.P., Weinberg, R.F., Dunlap, W.J., 1998. Transpressional tectonics along the Karakoram fault zone, northern Ladakh: constraints on Tibetan extrusion. In: Holdsworth, R.E., Strachan, R.A., Dewey, J.F. (Eds.), Continental Transpressional and Transtensional Tectonics. Geol. Soc., London, Spec. Pub., vol. 135, pp. 307–326.

Searle, M.P., Simpson, R.L., Law, R.D., Parrish, R.R., Waters, D.J., 2003. The structural geometry, metamorphic and magmatic evolution of the Everest massif, High Himalaya of Nepal–south Tibet. J. Geol. Soc., London 160, 345–366.

Shanker, R., Padhi, R.N., Arora, C.L., Prakash, G., Thussu, J.L., Dua, K.J.S., 1976. Geothermal exploration of the Puga and Chumathang geothermal fields, Ladakh, India. Proceedings, Second United Nations Symposium on the Development and Use of Geothermal Resources, San Francisco, USA, 20–29 May 1975, vol. 1. US Government Printing Office, Washington DC, pp. 245–258.

Simpson, R.L., Parrish, R.R., Searle, M.P., Waters, D.J., 2000. Two episodes of monazite crystallization during metamorphism and crustal melting in the Everest region of the Nepalese Himalaya. Geology 28, 403–406.

Solar, G.S., Pressley, R.A., Brown, M., Tucker, R.D., 1998. Granite ascent in convergent orogenic belts: testing a model. Geology 26, 711–714.

Unsworth, M.J., Jones, A.G., Wei, W., Marquis, G., Gokarn, S.G., Spratt, J.E., 2005. Crustal rheology of the Himalaya and southern Tibet inferred from magnetotelluric data. Nature 438, 78–81.

Valli, F., Arnaud, N., Leloup, P.H., Sobel, E.R., Mahéo, G., Lacassin, R., Guillot, S., Li, H., Tapponnier, P., Xu, Z., 2007. Twenty million years of continuous deformation along the Karakorum fault, western Tibet: a thermochronological analysis. Tectonics 26. doi:10.1029/2005TC001913.

Walker, J.D., Martin, M.W., Bowring, S.A., Searle, M.P., Waters, D.J., Hodges, K.V., 1999. Metamorphism, melting, and extension: age constraints from the High Himalayan slab of southeast Zanskar and northwest Lahaul. J. Geol. 107, 473–495.

Weinberg, R.F., Dunlap, W.J., Whitehouse, M., 2000. New field, structural and geochronological data from the Shyok and Nubra valleys, northern Ladakh: linking Kohistan to Tibet. In: Khan, M.A., Treloar, P.J., Searle, M.P., Jan, M.Q. (Eds.), Tectonics the Nanga Parbat Syntaxis and the Western Himalaya. Geol. Soc., London, Spec. Pub., vol. 170, pp. 253–275.

Weinberg, R.F., Sial, A.N., Mariano, G., 2004. Close spatial relationship between plutons and shear zones. Geology 32, 377–380.

Williams, I.S., 1998. U–Th–Pb geochronology by ion microprobe. Rev. Econ. Geol. 7, 1–35.

Wu, C., Nelson, K.D., Wortman, G., Samson, S.D., Yue, Y., Li, J., Kidd, W.S.F., Edwards, M.A., 1998. Yadong cross structure and South Tibetan Detachment in the east central Himalaya (89°–90°E). Tectonics 17, 28–45.

Zhang, H., Harris, N., Parrish, R., Kelley, S., Zhang, L., Rogers, N., Argles, T., King, J., 2004. Causes and consequences of protracted melting of the mid-crust exposed in the North Himalayan antiform. Earth Planet. Sci. Lett. 228, 195–212.